Combination therapy of glycation lowering compounds reduces caloric intake, improves insulin sensitivity, and extends lifespan.

Lauren Wimer[1], Kiyomi R. Kaneshiro[1], Jessica Ramirez[1], Martin Valdearcos[2], Muniesh Shanmugam[1], Dominique Gaffney[3], Parminder Singh[1], Jennifer Beck[1], Durai Sellegounder[1], Soo-Jin Cho[2], John Newman[1], James Galligan[3], Suneil Koliwad[2], Pankaj Kapahi[1]

[1] Buck Institute for Research on Aging, Novato, CA 94949
[2] The Diabetes Center, University of California San Francisco, San Francisco CA 94143
[3] University of Arizona, Tucson, AZ

Abstract:
Non-enzymatic reactions in glycolysis lead to the accumulation of methylglyoxal (MGO), a reactive precursor to advanced glycation end-products (AGEs), which has been suggested to drive obesity- and aging-associated pathologies. We observe that a combination of nicotinamide, lipoic acid, thiamine, pyridoxamine and piperine, which were selected to lower glycation (Gly-Low), reduce toxic glycolytic byproducts, MGO and MGO-derived AGE, MG-H1. Administration of Gly-Low reduced food consumption and body weight, improving insulin sensitivity and survival in both leptin receptor deficient (Lepr db) and wildtype C57 control mouse models. Unlike calorie restriction, Gly-Low inhibited ghrelin-mediated hunger responses and upregulated Tor pathway signaling in the hypothalamus. Gly-Low also extended lifespan when administered as a late life intervention, suggesting its potential benefits in ameliorating age-associated decline by inducing voluntary calorie restriction and reducing glycation.

Main Text
Despite the knowledge that obesity is a significant healthcare burden that reduces life expectancy by increasing the risk of several diseases, including diabetes, dementia, cardiovascular diseases, certain cancers, and severe COVID-19, the incidence of obesity is growing worldwide (*1, 2*). The increase in sugar intake is in part responsible for the obesity epidemic (*3*). Food overconsumption and obesity are also contributing factors to chronic hyperglycemia and enhanced glycolysis, which enhance the production of reactive a-dicarbonyls (a-DC's), such as methylglyoxal (MGO) (*4, 5*). MGO reacts nonenzymatically with biomolecules such as proteins, lipids, and DNA to form advanced glycation end-products (AGEs) (*6, 7*). These covalent adducts contribute to pathogenesis across several diseases by compromising protein function, forming extracellular crosslinks that disrupt tissue architecture, and modifying lipids and nucleic acids (*5*). Cellular protection against AGEs occurs by endogenous glyoxalase enzymes, which detoxify MGO and prevent AGEs formation (*4, 8*). Given that increased sugar consumption, which drives obesity, is accompanied by enhanced glycolysis and concomitant production of toxic glycolytic byproducts, we hypothesized that detoxification of AGEs may be a viable therapeutic against obesity and its associated pathologies.

To develop a therapeutic for AGEs burden we utilized compounds previously reported to reduce MGO (*9–13*). *In vitro* treatment of N27 cells with alpha lipoic acid,

nicotinamide, piperine, pyridoxamine, and thiamine was effective in rescuing neurite length retraction following exposure to MGO (Fig. S1A and Fig. S1B). The combination of these compounds, termed Gly-Low, displayed synergistic effects in protecting against MGO toxicity, and showed improvement compared to treatment with a single compound (Fig. S1C). *In vivo* treatment of C57BL/J6 control mice with Gly-Low resulted in significant lowering of body weights and food consumption compared to those on a control diet (Fig. 1A and 1B). Intraperitoneal injection of Gly-Low, as well as standard starving procedures, also reduced food consumption ruling out taste aversion as a potential caveat in reduction of food intake (Fig. S2A-S2D). Consistent with the role of carbohydrate utilization in driving MGO production, Gly-Low reduced food consumption on a high carbohydrate but not a high fat diet (Fig. S2E and S2F). Body composition testing revealed Gly-Low treatment led to a robust decrease in fat mass with preservation of lean mass (Fig. 1C). Reduced body weights and fat mass were found in conjunction with decreased random and fasted blood glucose levels (Fig. 1D). These decreased levels prompted us to explore the possibility of hyperinsulinemia through insulin tolerance testing (ITT) and glucose tolerance testing (GTT). Gly-Low treated mice demonstrated reduced blood glucose levels over time following an injection of D-glucose, as well as upon injection of insulin (Fig. 1E), suggesting an improvement in insulin sensitivity. Gly-Low treated mice also had increased energy expenditure as measured by heat production (Fig. 1F) and increased O_2 production (Fig. 1G) relative to kg of body weight, but no changes in respiratory exchange ratio (RER) (Fig. S2G) during a 60-hour metabolic cage test. Physical activity data from metabolic cages revealed equivalent movement, suggesting mice were not burning fat due to increased activity levels (Fig. 1H). Interestingly, Gly-Low treatment did not increase mRNA expression of thermogenic genes (e.g., *Ucp1, Pgc-1a*) in the brown adipose tissue (BAT) or liver tissue (Fig. S2H). This data taken together suggests that mice were not losing fat mass due to a shift from a carbohydrate burning state to that of fat-burning.
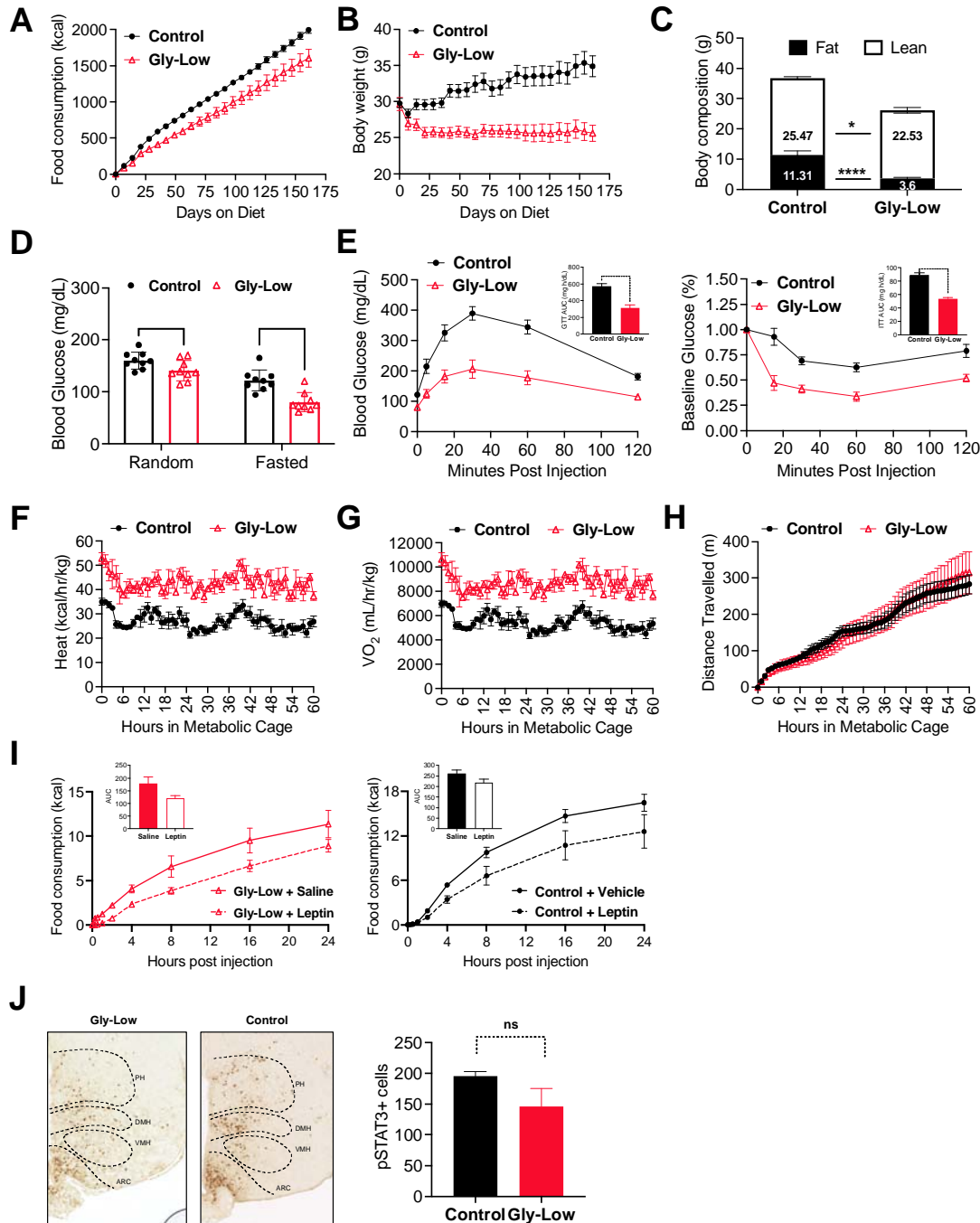
Figure 1. Glycation lowering compounds (Gly-Low) improve insulin sensitivity and reduce food consumption in a leptin independent manner.

A) Reduced cumulative food consumption in mice maintained on a Gly-Low supplemented diet (n = 9 per treatment group). B) Reduced body weight in mice maintained on a Gly-Low diet (n = 9 per treatment group). C) DXA scans demonstrated Gly-Low treated mice had sustained lean mass (g) and reduced fat mass (g) compared to control fed mice (n = 9 per treatment group). D) Random (non-fasted) and fasted (16h) blood glucose levels were decreased following Gly-Low treatment (n = 9 per treatment group). E) Gly-Low fed mice demonstrated increased glucose tolerance and increased insulin sensitivity demonstrated by decreased blood glucose levels following an IP injection of glucose (2g/kg BW) (left) and decreased baseline glucose levels (%) following an IP injection of insulin (0.75 U/kg BW) (right). Bar graph quantification are mean AUC levels +/- SEM (n = 6 per treatment group). F) Increased energy expenditure in Gly-Low treated mice during a 60-hour singly housed metabolic cage run (normalized to kg initial body weight) (n = 3-5 per treatment group). G) Increased oxygen consumption in Gly-Low treated mice during a 60-hour singly housed metabolic cage run (normalized to kg initial body weight) (n = 3-5 per treatment group). H) Equivalent distance traveled between Gly-Low fed and control fed mice during a 60-hour singly housed metabolic cage run (n = 3-5 per treatment group). I) Food consumption rates of Gly-Low fed (left, red) and control fed (right, black) mice following an injection of either leptin or a saline vehicle. Bar graph quantification are mean AUC values +/- SEM (n = 7 per treatment group). J) Representative sections showing statistically similar pSAT3 staining in the hypothalamus mice 45 min after leptin injection (3 mg/kg) (n = 3). All data are presented as mean +/- SEM. Analyzed by student t-test, two-tailed, equal variance. * $p < 0.05$, **$p < 0.01$, ***$p < 0.001$, ****$p < 0.0001$.

Due to its effect on feeding and energy homeostasis, we tested whether Gly-Low's effect on feeding was mediated by leptin, the hormone responsible for satiety signaling. Intraperitoneal (IP) leptin injections of Gly-Low and control fed mice resulted in decreased food intake relative to saline injected controls, with statistically similar area under the curve (AUC) analyses (**Fig. 1I**). Additionally, leptin-induced STAT3 activation in hypothalamic neurons was unchanged in Gly-Low mice compared to control-fed mice following an IP injection of leptin (**Fig. 1J**), suggesting no change in leptin responsiveness. These data suggest Gly-Low reduced food intake independent of the leptin pathway.

To further examine the interaction between Gly-Low and leptin we determined the effect of Gly-Low on food intake in a hyperphagic leptin receptor deficient (Lepr db) mouse model. We tested varying concentrations of Gly-Low and found a dose-dependent effect on body weights and food consumption (**Figs. 2A, 2B, S3A and S3B**). Due to the effectiveness of the highest dose, we restricted further analyses to this concentration. Similar to wildtype mice, Gly-Low treated Lepr db mice demonstrated fat mass-related weight loss (**Fig. 2C**) and increased metabolic energy expenditure without any apparent changes in gross motor activity (**Fig. 2D and Fig 2F**). Gly-Low treated mice also showed similarly increased VO_2 (**Fig. 2E**) levels, but no changes in respiratory exchange ratio (RER) (**Fig. S3C**). Several obesity-associated pathologies characteristic of the Lepr db mouse model were significantly decreased upon Gly-Low treatment, such as blood glucose levels (**Fig. 2G**) and liver lipid accumulation (**Fig. 2H**). Gly-Low

treatment rescued the lifespan deficits witnessed in their untreated controls by the time of sacrifice (**Fig. 2I**) and mitigated diabetic complications such as peripheral neuropathy and increased urination (**Fig. S3D and S3E**). Moreover, Gly-Low treatment significantly reduced diabetes and obesity-associated glycolytic metabolite, MGO, as well as its protein-bound arginine adduct, MG-H1 (**Fig 2J**). Together these findings support the hypothesis that glycation lowering compounds can reduce obesity and its associated pathologies.

Next, we undertook an omics approach to elucidate the metabolic impact of acute Gly-Low treatment on wildtype mice (**Fig. 3A**). Metabolic profiling of plasma from Gly-Low treated mice revealed a significant decrease in glycolytic intermediates and an increase in products of the pentose phosphate pathway (PPP) (**Fig. 3B**). KEGG analysis of significantly increased metabolites revealed the most robust upregulation of the Pentose Phosphate Pathway (PPP) as well as increases in the nicotinamide metabolism and vitamin B6 metabolism pathways (**Fig. 3C**), which was attributed to the presence of nicotinamide and pyridoxamine in Gly-Low. Next, we sought to identify changes within the hypothalamus using RNA sequencing analysis, given its critical role in signaling hunger and satiety, as well as producing pro-hormones to regulate feeding and nutrient acquisition (*14, 15*). Transcript analysis revealed 10,359 differentially expressed genes (p adj < 0.05) from 28,226 protein coding genes (**Fig. 3D**) between Gly-Low treated and untreated mice. Consistent with our plasma metabolomics findings, in the hypothalamus, Gly-Low treatment reduced genes involved in glycolysis (**Fig. 3E**) and increased those in the pentose phosphate pathway (**Fig. 3F**) and MGO detoxification (**Fig. 3G**). Together, these changes are consistent with lowering of MGO, through reduction of glucose utilization and enhanced detoxification.
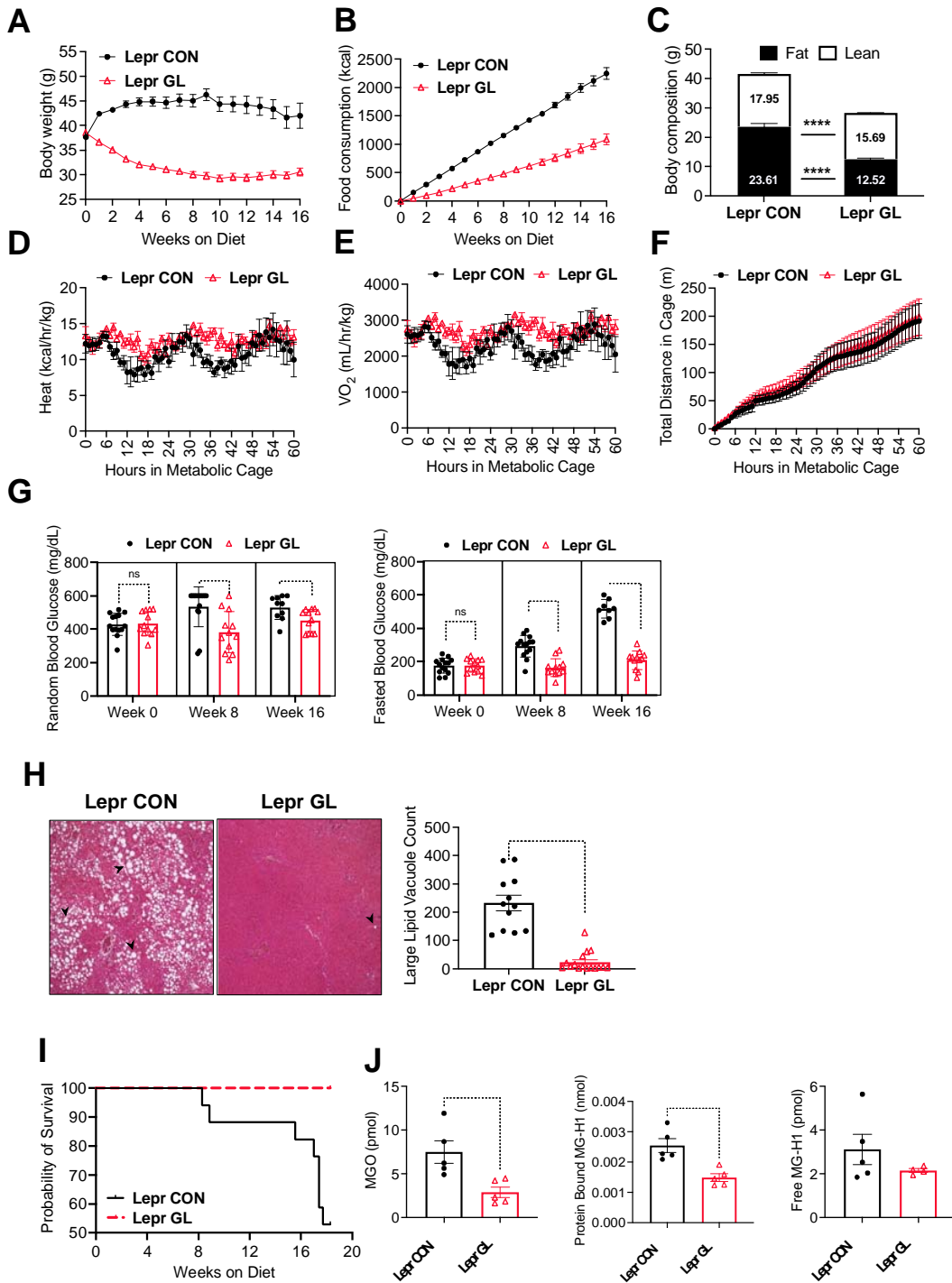
Figure 2. Gly-Low rescues hyperphagia and obesity in a leptin receptor deficient mouse model

A) Reduced food consumption in Lepr mice fed a Gly-Low supplemented diet (n = 12 – 17 per treatment group). B) Reduced body weight in Lepr mice fed a Gly-Low diet (n = 12 -17 per treatment group). C) DXA scans demonstrated Gly-Low treated Lepr mice

had sustained lean mass (g) and reduced fat mass (g) compared to control fed mice (n = 8-12). D) Equivalent energy expenditure in Gly-Low treated Lepr mice during a 60-hour singly housed metabolic cage run (normalized to kg initial body weight) (n = 4 per treatment group). E) Equivalent oxygen consumption in Gly-Low treated Lepr mice during a 60-hour singly housed metabolic cage run (normalized to kg initial body weight) (n = 4 per treatment group). F) Equivalent distance traveled between Gly-Low fed and control fed Lepr mice during a 60-hour singly housed metabolic cage run (n = 4 per treatment group). G) Random (non-fasted) (left) and fasted (16h) blood glucose levels (right) were decreased in Lepr mice treated with Gly-Low throughout the length of the study (week 8 and week 16) (n = 8-12 per treatment group). H) Representative sections showing reduced large lipid vacuoles (black arrows) in the livers of Gly-Low treated Lepr mice (left). Quantification of large lipid vacuoles between treatment groups (right). (n = 3-4 mice per treatment group, 3 fields per liver section). I) Kaplan-Meier curve of obesity-related disease mortality in Lepr mice fed a control chow diet and a Gly-Low supplemented diet (n = 12-17). J) Mass spectrometry quantification of free MGO, protein-bound MG-H1, and free MG-H1 in the plasma of Lepr mice (n = 5). All data are presented as mean +/- SEM. Analyzed by student t-test, two-tailed, equal variance. * $p < 0.05$, **$p < 0.01$, ***$p < 0.001$, ****$p < 0.0001$.

On one hand, Gly-Low treated mice have reduced calorie intake which leads to phenotypes akin to calorie restriction, however unlike calorie restriction the mice have reduced hunger and initiate the restriction of calories voluntarily. Unlike calorie restriction, Gly-Low reduces gluconeogenesis. RT-qPCR analysis of liver tissue from Gly-Low treated mice confirmed decrease in gluconeogenesis genes, glucose 6 phosphatase (*G6P*) and phosphoenolpyruvate kinase 1 (*Pck1*) (**Fig. 3H**). Key feeding genes *Agrp* and *Pomc* were differentially expressed in the same direction as seen during hunger. To further examine the relationship between calorie restriction and Gly-Low treatment, we compared significant gene expression changes from the hypothalami of Gly-Low treated mice *versus* published datasets from the hypothalmi of calorically restricted (CR) (**Fig. 1J** (left)) and food restricted (FR) mice (**Fig. 1J** (right)) (*16*). Linear regression analysis of our data set against both the CR and FR datasets revealed genes that were both positively and negatively correlated. This is consistent with the idea that Gly-Low treated mice show pleiotropic effects, they have reduced calorie intake but also increased satiety.

Analysis of the oppositely altered differentially expressed genes revealed clustering within genes associated with Tor activation and ribosomal translation (**Fig. S4A**). During nutrient deprivation, such as in CR, the TOR growth signaling pathway is inhibited and protein synthesis is reduced. Surprisingly, genes associated with TOR signaling were upregulated in the hypothalami of Gly-Low treated mice despite their reduced food consumption. Transcripts revealed mTOR activator, *Rheb*, was significantly upregulated while *Rheb* inhibitors, *Tsc1/Tsc2,* were significantly downregulated (**Fig. S4B**). Within the mouse hypothalamus, Tor activation partially occurs through stimulation of the growth hormone receptor (Ghr) and inhibition of the growth hormone secretagogue receptor (Ghsr) (**Fig. 4A**) (*17, 18*). Ghr binding promotes AKT phosphorylation to induce Tor activation, while Ghsr binding promotes AMPK phosphorylation to inhibit Tor

activation and downstream S6 Kinase phosphorylation. Hypothalamic lysates of Gly-Low treated mice showed reduced pAMPK expression, equivalent pAKT expression, and increased pS6 expression relative to their non-phosphorylated counterparts (**Fig. 4B**). Taken together, this data suggests that Tor activation occurs through reduced inhibition by pAMPK downstream of Ghsr signaling. To determine why Gly-Low mice had reduced Ghsr activation, we investigated plasma levels of ligands which bind the Ghsr. We investigated levels of Ghrelin, the hormone responsible for activating Ghsr, and found there was no significant change between treatment groups (**Fig. 4C**). We also found levels of LEAP2, the hormone responsible for antagonizing Ghsr, were significantly reduced with Gly-Low treatment, suggesting there was no competitive binding for the receptor (**Fig. 4D**). Mice typically demonstrate increased levels of ghrelin and decreased levels of LEAP2 during fasting (**Fig. S4C**). Gly-Low treatment also reduced levels of IGF-1, a hormone produced downstream of effective ghrelin-Ghsr binding (**Fig. 4E**). Ghrelin is well known as the hunger hormone, and with appropriate binding, produces feelings of hunger and food-seeking behavior in mammals (*19*). Upon an injection with ghrelin, control mice exhibited increased food consumption compared to their vehicle injected controls, while Gly-Low treated mice failed to respond to the exogenous ghrelin (**Fig. 4F**). Together, these data suggest that Gly-Low blunts ghrelin responses both molecularly and physiologically.
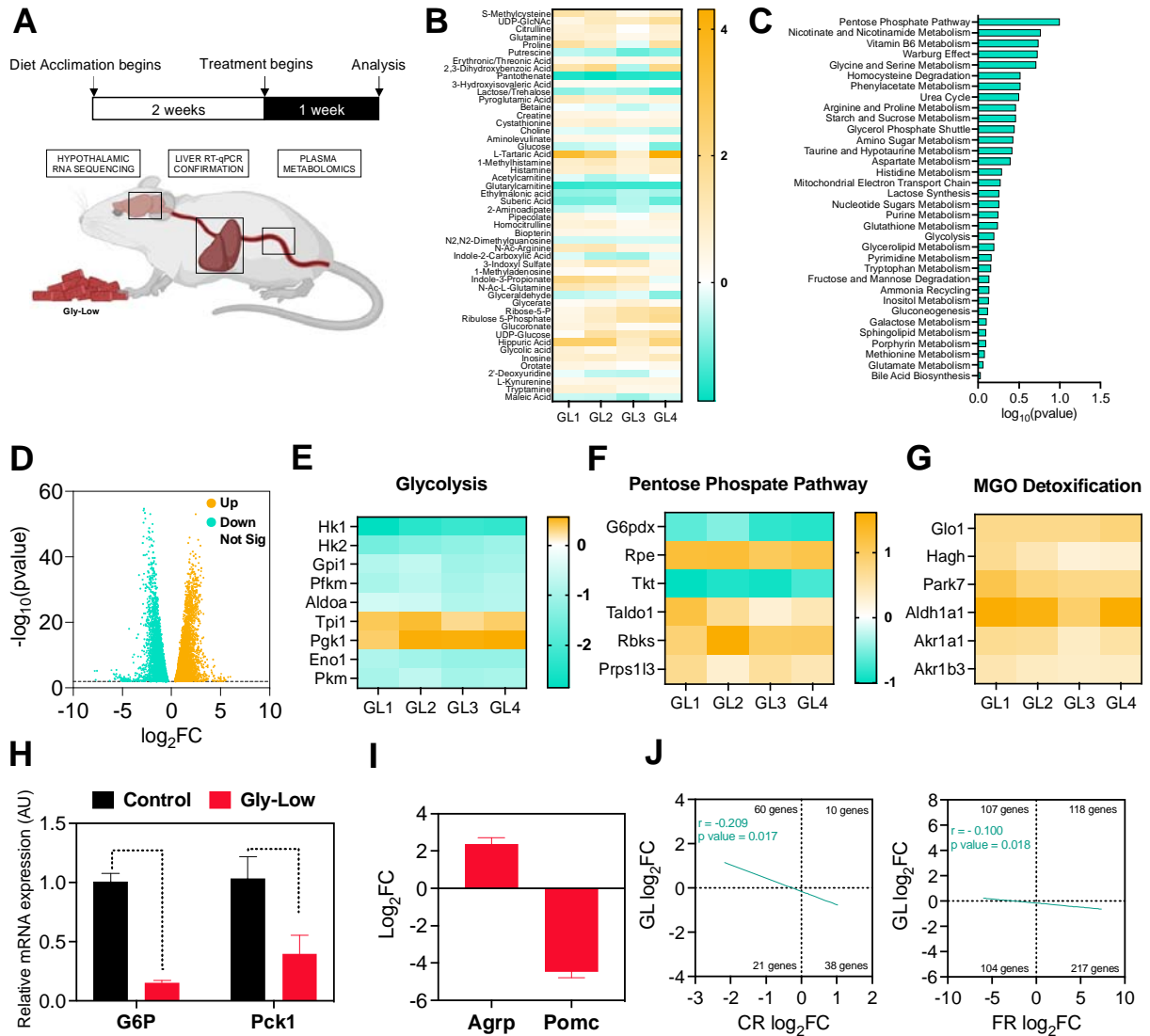
Figure 3. Gly-Low reprograms metabolism to reduce glycolysis, enhance MGO detoxification and increase mTor signaling in the hypothalamus.
A) Experimental design and strategy to quantify alterations caused by Gly-Low treatment. Hypothalamic rna sequencing, plasma metabolomics, and RT-qPCR verification was performed following an acute treatment (7 days) of Gly-Low diet. B) Heatmap of significantly altered ($p < 0.05$) metabolites within the plasma (n = 4). C) Categorization of metabolic pathways associated with the list of significantly ($p < 0.05$) up-regulated metabolites with Gly-Low treatment. D) A volcano plot of differentially expressed genes between mice treated acutely (7 days) with Gly-Low and control fed mice. Blue dots are genes significantly down regulated ($p < 0.01$) in Gly-Low relative to control. Orange dots are genes significantly upregulated ($p < 0.01$) in Gly-Low relative to

control (n = 4). E) Heatmap of significantly altered genes *(p < 0.01)* responsible for enzymes involved in glycolysis. F) Heatmap of significantly altered genes ($p < 0.01$) responsible for enzymes involved in the pentose phosphate pathway. G) Heatmap of significantly altered genes ($p < 0.01$) involved in the detoxification of methylglyoxal. H) Significant alterations in prominent feeding genes, *Agrp* and *Pomc* with Gly-Low treatment. I) Reduced expression of gluconeogenesis genes, *G6p* and *Pck1,* quantified by RT-qPCR (n = 3-4). J) Scatterplot of log2 fold changes of genes significantly ($p < 0.01$) altered in the hypothalamus of Gly-Low treated mice plotted against log2 fold changes of genes significantly altered ($p < 0.05$) in the hypothalamus of calorie restricted (50% CR) mice (left). Scatterplot of log2 fold changes of genes significantly ($p < 0.01$) altered in the hypothalamus of Gly-Low treated mice plotted against log2 fold changes of genes significantly altered ($p < 0.05$) in the hypothalamus of food restricted (24h) mice. The regression line is shown in blue. The Pearson correlation coefficient, R, and p values are shown in the top right. Numbers of genes in each quadrant are shown. All data are presented as mean +/- SEM. Analyzed by student t-test, two-tailed, equal variance. * $p < 0.05$, **$p < 0.01$, ***$p < 0.001$, ****$p < 0.0001$. Scatterplots analyzed by simple linear regression.

Finally, we explored the late life benefits of decreased hunger signaling and reduced calorie intake by administering Gly-Low to aged C57BL/6 mice. Survival analysis demonstrated control mice lived a median of 825 days (105 days after beginning dietary intervention) while Gly-Low treated mice lived a median of 888 days (173 days after beginning dietary intervention) (**Fig. 4G**). This extension in lifespan was an 8.25% increase in median lifespan (p value = 0.0199, Mantel-Cox) and a 5.23% increase in maximum lifespan. RNA sequencing of the hypothalamus of aged Gly-Low treated mice (25 mos) demonstrated a shift in gene expression more toward that of a young mouse (3 mos) compared to that of an age matched control (25 mos) (**Fig. 4H**). Furthermore, aged Gly-Low treated mice also retained youthful metabolic phenotypes such as increased insulin sensitivity and reduced glucose levels (**Unpublished data, Kapahi Lab**).

Methylglyoxal has been suggested as a critical target for aging and age-related diseases which has been a challenge to target pharmacologically (*20*). We demonstrate that Gly-Low reduces MGO and its glycation product, MG-H1, by multiple mechanisms including reduction of glycolysis and increase in detoxification. Furthermore, we demonstrate that Gly-Low reduces MGO, and has both short term and long-term physiological consequences by reducing appetite, lowering body weight, increasing insulin sensitivity, and extending lifespan. A prior study showed that MGO modified bovine serum albumin fed mice showed insulin resistance, increased body weight and shortened lifespan (*21*). These results are also consistent with a clinical trial using glyoxalase activating compounds that demonstrated reduced weight and insulin resistance (*22*).

Calorie restriction has been shown to improve metabolic health and slow aging and age-related diseases in multiple species (*23*). However, long term calorie restriction is not sustainable in humans. Therefore, development of interventions that allow voluntary calorie restriction hold promise to enhance healthspan. Gly-Low treatment differs from calorie restriction in multiple ways. Gly-Low treated mice demonstrate satiety despite reduced calorie intake in part by blocking the effects of ghrelin and enhancing Tor signaling in the hypothalamus. Unlike calorie restriction, Gly-Low is quite effective at extending lifespan even late in life, which might be in part due to improved metabolic flexibility as seen by improved insulin sensitivity (*24*). Thus, reducing MGO induced glycation could serve as an effective therapeutic to improve metabolic health and slow aging and age-related diseases.
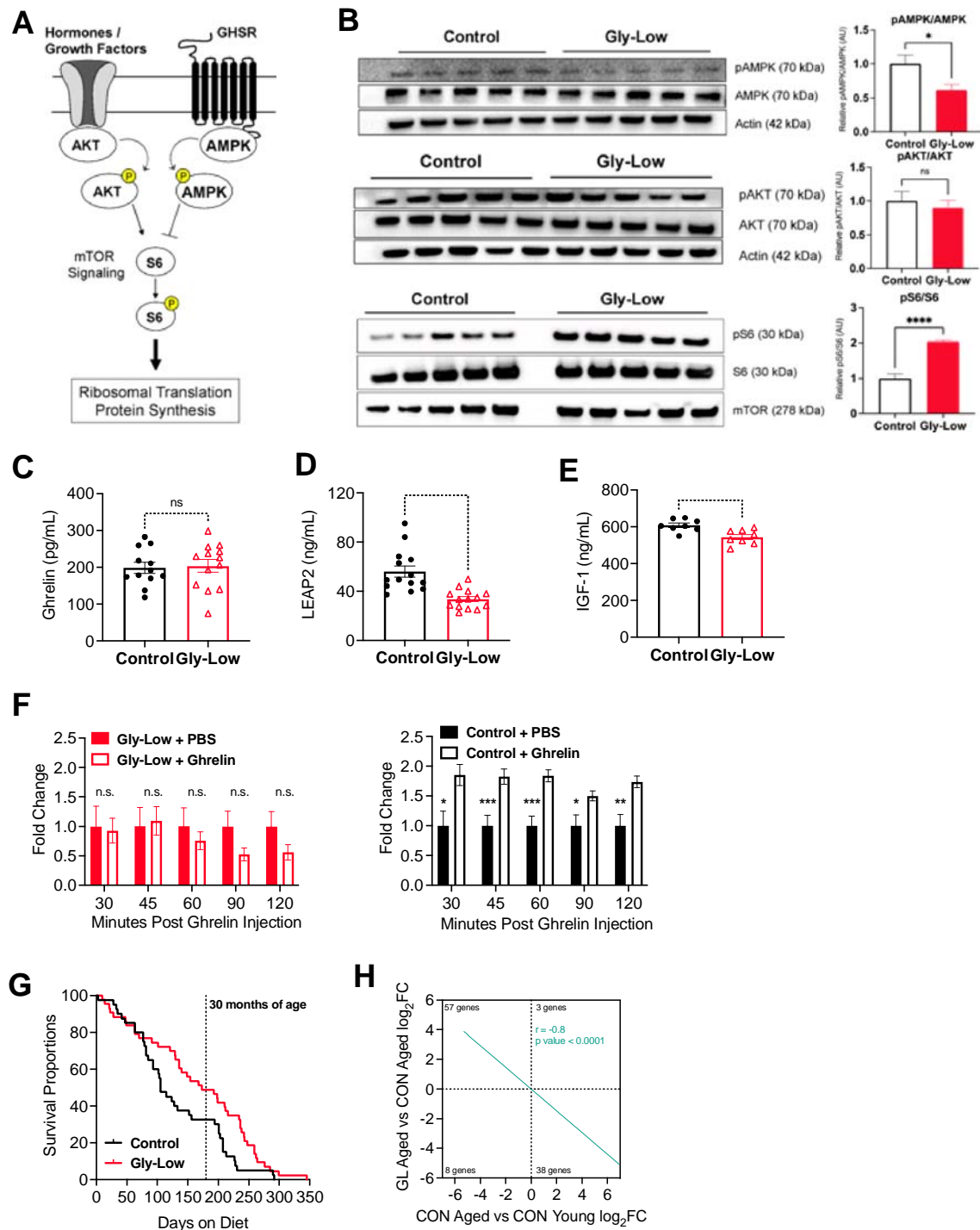
Figure 4. Gly-Low compounds enhance Tor activation and inhibit ghrelin responsiveness in the hypothalamus.

A) Schematic of Tor activation in response to ghrelin and growth hormone within the hypothalamus. B) Expression levels of upstream activators and inhibitors of Tor activation, and downstream activation was determined by western blot of hypothalamic lysates (left). Actin was used as a loading control. Quantification of band intensity (right). C) Equivalent levels of ghrelin, the GHSR binding hormone, in the plasma of Gly-Low treated and control mice (n = 12-13). D) Reduced levels of LEAP2, a GHSR endogenous antagonist, in the plasma of Gly-Low treated mice (n = 14 per treatment group). E) Gly-Low fed mice demonstrated significantly reduced plasma IGF-1 levels (n = 8 per treatment group). F) Log2 fold changes of primary feeding genes, *agrp* and *pomc* in the hypothalamus of Gly-Low fed mice. G) Fold changes of food intake over time in Gly-Low fed (left) and control fed (right) mice injected with 0.1 mg/kg ghrelin normalized to PBS injections. Gly-Low treated mice demonstrated no change in food intake when challenged with ghrelin injections, while control chow fed mice showed increased consumption (n = 5 per treatment group). H) Kaplan-Meier curve of aged (24 mo) of age-related disease mortality in mice fed a control chow diet and a Gly-Low supplemented diet (n = 42-43 per treatment group). I) Scatterplot showing the log2 fold changes of genes significantly (p value < 0.05) altered in the hypothalamus of Gly-Low treated (25 mo fed Gly-Low for 5 months vs 25 mo fed chow control) and aged (25 mo fed control chow vs 3 mo fed control chow) mice. The regression line is shown in blue. The Pearson correlation coefficient, R, and pvalues are shown in the top right. Numbers of genes in each quadrant are shown. All data are presented as mean +/- SEM. Analyzed by student t-test, two-tailed, equal variance. * p < 0.05, **p < 0.01, ***p < 0.001, ****p < 0.0001. Scatterplots analyzed by simple linear regression.

Methods

Mice

Studies included the use of male C57BL/6J (Jackson Laboratories #000664) control mice, male leptin receptor deficient mice (Jackson Laboratories #000642, homozygous for Lepr^{db}, wild type for Dock7^m) aged between 8 and 12 weeks, as well as 19-month-old male C57BL/6J mice (National Institutes of Aging, Bethesda, MD). All mice were communally housed and age-matched with *ad libitum* access to water and diet in a pathogen and temperature-controlled room with a 12h light-dark cycle beginning at 06:00 AM. All procedures were conducted in accordance with NIH Guidelines for Care and Use of Animals and were approved by the Institutional Animal Care and Use Committees at Buck Institute for Research on Aging and the University of California San Francisco.

Experimental Diets

Mice were fed either a standard low-fat chow diet (21% fat (kcal), 60% carbohydrate (kcal) Envigo: TD.200743), a standard high fat chow diet (60% fat (kcal), 21% carbohydrate (kcal), Envigo: TD.200299), a standard low-fat chow diet supplemented with our Gly-Low compound cocktail (21% fat (kcal), 60% carbohydrate (kcal) Envigo: TD.200742), or a standard high fat chow diet supplemented with our Gly-Low compound cocktail (60% fat (kcal), 21% carbohydrate (kcal).

A combination of supplemental grade compounds, safe to be consumed in set dosages, were prepared and incorporated into a modified pre-irradiated standard AIN-93G mouse chow diet from Envigo. The cocktail consists of alpha lipoic acid (20.19%), nicotinamide (57.68%), thiamine hydrochloride (4.04%), piperine (1.73%), and pyridoxamine dihydrochloride (16.36%), and is supplemented in the diet to achieve a daily consumption rate in mg/kg of body weight/day. Noted vocabulary where 1X is equal to a full dose, 0.5X is equal to half dose, and 0.25X is equal to a quarter dose of the compound cocktail.

Lifespan

19-month-old male C57BL/6J mice received from National Institutes of Aging (Bethesda, MD) and maintained on vivarium chow until they reached 24 months of age. At 24 months of age, mice were randomly assigned to begin either a control chow diet or Gly-Low diet. Health checks were performed 5 times a week and mice reached either a humane endpoint or died of natural causes.

Measuring Food Intake and Energy Metabolism

Food consumption and body weights were weighed once weekly. Chow weight of communally caged mice was recorded once weekly and individual intake was measured as change in weight over the week divided by the number of mice per cage.

Metabolic parameters in mice were assessed using a Promethion Metabolic Caging System housed in the Buck Institute Mouse Phenotyping Core. Mice were singly housed and received water and food *ad libitum*. Cages were maintained at 20°-22° C under a

12h light-dark cycle beginning at 06:00 AM, and mice were acclimated to single housing 24h before being studied. The cages continuously weighted food for each mouse, and daily intake was measured as change in food weight over 24h periods. Metabolic data was collected by respiration rates of each mouse and was normalized to individual mouse body mass. X, Y, and Z beam breaks quantified total activity and steps taken during the metabolic cage run.

Body Composition Quantification
Echo MRI and DXA scans were used to analyze body composition in anesthetized (isoflurane) immobilized mice. Water weight and bone mass were excluded from body weight to quantify lean and fast mass.

Glucose Testing
Random (non-fasted) and fasted blood glucose levels were determined for each mouse. Non-fasted blood glucose levels were assessed between 08:00AM and 10:00AM by a collection of blood by tail nick and the use of a handheld glucometer (AccuCheck). Fasted blood glucose was determined after a 16h fast between 8:00AM and 10:00AM by a collection of blood by tail nick and the use of a handheld glucometer (AccuCheck).

Glucose and Insulin Tolerance Testing
Food was removed from control fed and Gly-Low fed mice 14 hr prior to testing of glucose tolerance from 6:00 PM to 8:00 AM. Mice received IP injections of D-glucose (2 mg/kg), followed by a single tail nick to collect blood for blood glucose monitoring by handheld glucometer (AccuCheck). Total glucose AUC was measured by Graphpad Analysis.

Food was removed from control fed and Gly-Low fed mice 4 hr prior to testing of insulin tolerance from 8:00 AM to 12:00 PM. Mice received IP injections of insulin (0.75U/kg), followed by a single tail nick to collect blood glucose monitoring by handheld glucometer (AccuCheck). Total glucose AUC was measured by Graphpad Analysis.

Ghrelin Responsiveness
Ghrelin peptides (Catalog #031-30)(Phoenix Pharmaceuticals, Inc.). Mice were injected with reconstituted ghrelin (0.1 mg/kg) by subcutaneous injection. Following injection, mice were singly housed, and individual food consumption was recorded over 90 minutes post-injection.

Hormone Quantification:
Blood samples were collected by cardiac puncture when mice were euthanized for dissection. Blood samples were collected in heparin lined tubes and left on ice for 30 min. Afterward, samples were centrifuged for 15 min at 2200 g to isolate plasma. Ghrelin, LEAP2, and IGF-1 were measured in plasma by ELISA kits according to manufacturer's instructions.
LEAP2 ELISA (Catalog #075-40) (Phoenix Pharmaceuticals, Inc.)
Ghrelin ELISA (EZRGRA-90K)(Sigma Aldrich)
IGF-1 ELISA (Catalog #80574) (Crystal Chem)

Hypothalamic RNA Sequencing:
19-month-old male C57BL/6J mice were ordered from the National Institutes of Aging (Bethesda, MD). Mice were fed vivarium chow (Envigo Teklad 2018) before starting either a control diet or Gly-Low diet at 20 months of age. After 5 months on diet, 5 mice per group were sacrificed via CO_2 asphyxiation followed by cervical dislocation. The brain was rapidly dissected, and hypothalamus removed with tweezers, flash frozen and stored at -80˚C. RNA was isolated using Zymo research quick RNA miniprep kit (cat # 11-328) according to manufacturer's recommendations. Isolated RNA was sent for library preparation and sequencing by Novogene Corporation Inc. where RNA was poly-A selected using poly-T oligo-attached magnetic beads, fragmented, reverse transcribed using random hexamer primers followed by second strand cDNA synthesis using dTTP for non-directional library preparation. Samples underwent end repair, A-tailing, adapter ligated, size selected, amplified, and purified. Illumina libraries were quantified using Qubit and qPCR and analyzed for size distribution using bioanalyzer. Libraries were pooled and sequenced on Illumina platforms (). Data quality was assessed, and adaptor reads and low-quality reads were removed. Reads that passed the quality filtering process were mapped paired end to the reference genome (GRCm38) using Hisat2 v2.0.5. featureCounts v1.5.0-p3 was used to count reads that mapped to each gene. Differential expression analysis was performed using DESEq2 (1.20.0).

Histology and immunocytochemistry:
Mice were euthanized with CO_2 asphyxiation and cervical dislocation. Dissections were performed and mouse brains were removed and washed with PBS before being postfixed in 4% PFA overnight with agitation at 4C. Afterwards, a brain matrix (BrainTree) was used to isolate sections containing the hypothalamus. This section was immediately embedded in OCT, frozen on dry ice, and stored at -80C. Next, 35-micron sections were cut on a cryostat, blocked for 1 hr with 5% BSA containing 0.1% triton X-100, and incubated with pSTAT3 (1:200, Cell Signaling). Adequate secondary antibody was used for the HRP-diaminobenzidine reaction. The HRP-diaminobenzidine reaction was performed using the ABC Kit (Vector Laboratories), using biotin-labeled goat anti-rabbit IgG. Images were acquired using a Zeiss AxioImager brightfield microscope.

Dissections were performed and mouse livers were removed and washed with PBS before being postfixed in 4% PFA overnight with agitation at 4C. Afterwards, livers were moved to 70% EtOH prior to being paraffin embedded and sectioned. The liver was sectioned by microtome in a coronal orientation at a thickness of 4 microns. H&E staining and trichrome staining was used for identification and quantification of large lipid vacuoles.

RT-PCR:
Total RNA was extracted using Trizol (Invitrogen), purified with RNeasy Mini-Kit (Qiagen) according to manufacturer's instructions, and reverse transcribed using iScript Reverse Transcription Supermix (BioRad). cDNA was subjected to PCR analysis with

gene-specific primers in the presence of SyGreen Blue Mix (Genesee). Relative mRNA abundance was obtained by normalization to actin and tubulin housekeeping genes.

Western Blotting:

Proteins were extracted from hypothalamic samples in TPER buffer (Thermo Fisher) containing a protease inhibitor cocktail (Sigma). Protein extracts were denatured at 70C for 15 min prior to running on a 5-12% Bi-Tris gel. Transfer was completed using iBlot (Thermo Fisher) and blocked in 5% BSA for 1 hr. Primary antibodies were incubated overnight at 4C with agitation. Adequate HRP-conjugated antibodies were incubated at room temperature for 1 hr prior to imaging.

Akt (Cell Signaling)(40D4) 1:1000
pAKT Ser473 (Cell Signaling)(D9E) 1:1000
s6: (Cell Signaling) (5G10) (2217) 1:1000
ps6 Ser 240/244: (Cell Signaling) (D68F8) 1:1000
AMPK: (Cell Signaling) (CST-4181) 1:1000
pAMPK: (Cell Signaling) (CST-2531)
Actin (Cell Signaling) (13E5) 1:1000

Mass Spectrometry MGO Quantification:

Quantification of Dicarbonyls. 200 µL of 80:20 MeOH:ddH$_2$O (-80°C) containing 50 pmol ^{13}C$_3$-MGO was added to 10 µL of serum and extracted at -80°C overnight. Insoluble protein was removed via centrifugation at 14,000 x g for 10 min at 4°C. Supernatants were derivatized with 10 µL of 10 mM o-phenylenediamine for 2 h with end-over-end rotation protected from light (Galligan et al., 2018). Derivatized samples were centrifuged at 14,000 x *g* for 10 min and the supernatant was chromatographed using a Shimadzu LC system equipped with a 150 x 2mm, 3µm particle diameter Luna C$_{18}$ column (Phenomenex, Torrance, CA) at a flow rate of 0.450 mL/min. Buffer A (0.1% formic acid in H$_2$O) was held at 90% for 0.25 min then a linear gradient to 98% solvent B (0.1% formic acid in acetonitrile) was applied over 4 min. The column was held at 98% B for 1.5 min and then washed at 90% A for 0.5 min and equilibrated to 99% A for 2 min. Multiple reaction monitoring (MRM) was conducted in positive ion mode using an AB SCIEX 4500 QTRAP with the following transitions: *m/z* 145.1→77.1 (MGO); *m/z* 235.0→157.0 (3-DG); m/z 131.0→77.0 (GO); m/z 161.0→77.0 (HPA); m/z 148.1→77.1 (^{13}C$_3$-MGO, internal standard).

Quantitation of PTMs (QuarkMod). Protein pellets from the dicarbonyl quantifications (above) were resuspended in 65 µL of 50 mM NH$_4$HCO$_3$, pH 8.0. Samples were spiked with 10 µL of a master mix containing internal standards (see table). Proteins were digested via the addition of 5 µL of sequencing grade trypsin (0.1 mg/mL) (Promega) for 3 h at 37 °C. Trypsin was denatured via boiling at 95 °C for 10 min and samples were cooled to room temperature. Aminopeptidase M (Millipore, 15 µg in 10 µL) was added and samples were incubated overnight at 37°C. Aminopeptidase was denatured via heating at 95 °C for 10 min and samples were again cooled to room temperature. 15 µL of heptafluorobutyric acid (1:1 in H$_2$O) was added to each sample and debris was removed via centrifugation at 14,000 × *g* for 10 min. Clarified supernatants were chromatographed using a Shimadzu LC system equipped with a 150 x 2.1mm, 3.5 mm particle diameter Eclipse XDB-C8 column (Agilent, Santa Clara, CA) at a flow rate of

0.4500 mL/min. Mobile phase A: 10 mM HFBA in water; mobile phase B: 10 mM HFBA in ACN. The following gradient was used: 2 min, 1% B; 6 min, 50% B; 6.5 min, 95% B; 9 min 95% B; 9.5 min, 1% B. The column was equilibrated for 3 min at 5% B. MRM was conducted in positive mode using an AB SCIEX 4500 QTRAP. The MRM detection window was 50 sec with a target scan time of 0.75 sec. The following parameters were used for detection and as previously described (Gaffney et al., 2020; Galligan et al., 2017):

Species	Q1 (*m/z*)	Q3 (*m/z*)	CE (V)
Lys	147.1	84.1	29
$^{13}C_6{}^{15}N_2$ Lys	155.1	90.1	29
Arg	175.1	70.1	47
$^{13}C_6{}^{15}N_4$ Arg	185.1	75.1	47
Leu	132.1	86.1	17
$^{13}C_6{}^{15}N$ Leu	139.1	93.1	17
MG-H1	229.2	70.1	53
^{13}C-MG-H1	230.2	70.1	53
CEA	247.2	70.1	55
^{13}C-CEA	248.2	70.1	55
CEL	219.2	84.1	41
CEL-d_4	223.2	88.1	41
CML	205.0	84.1	38

CML-d$_4$	209.0	88.1	38

Quantification of free MGH1. 10 µL of serum was added to 200 µL of 80:20 MeOH:ddH$_2$O (-80°C) containing 10 pmol ^{13}C-MG-H1 and extracted at -80°C overnight. Insoluble protein was removed via centrifugation at 14,000 x g for 10 min at 4°C and supernatants were transferred to a new tube. 15 µL of heptafluorobutyric acid (1:1 in H$_2$O) was added to each sample and debris was removed via centrifugation at 14,000 × g for 10 min. Samples were analyzed as described above (QuARKMod).

References

1.   M. Blüher, Obesity: global epidemiology and pathogenesis. *Nat. Rev. Endocrinol.* **15**, 288–298 (2019).

2.   B. M. Popkin, S. Du, W. D. Green, M. A. Beck, T. Algaith, C. H. Herbst, R. F. Alsukait, M. Alluhidan, N. Alazemi, M. Shekar, Individuals with obesity and COVID-19: A global perspective on the epidemiology and biological relationships. *Obes. Rev.* **21**, e13128 (2020).

3.   R. J. Johnson, L. G. Sánchez-Lozada, P. Andrews, M. A. Lanaspa, Perspective: A Historical and Scientific Perspective of Sugar and Its Relation with Obesity and Diabetes. *Adv. Nutr.* **8**, 412–422 (2017).

4.   I. Allaman, M. Bélanger, P. J. Magistretti, Methylglyoxal, the dark side of glycolysis. *Front. Neurosci.* **9**, 23 (2015).

5.   C. G. Schalkwijk, C. D. A. Stehouwer, Methylglyoxal, a Highly Reactive Dicarbonyl Compound, in Diabetes, Its Vascular Complications, and Other Age-Related Diseases. *Physiol. Rev.* **100**, 407–461 (2020).

6.   G. Vistoli, D. De Maddis, A. Cipak, N. Zarkovic, M. Carini, G. Aldini, Advanced glycoxidation and lipoxidation end products (AGEs and ALEs): an overview of their mechanisms of formation. *Free Radic. Res.* **47 Suppl 1**, 3–27 (2013).

7.   J. Bellier, M.-J. Nokin, E. Lardé, P. Karoyan, O. Peulen, V. Castronovo, A. Bellahcène, Methylglyoxal, a potent inducer of AGEs, connects between diabetes and cancer. *Diabetes Res. Clin. Pract.* **148**, 200–211 (2019).

8.   D. E. M. Maessen, C. D. A. Stehouwer, C. G. Schalkwijk, The role of methylglyoxal and the glyoxalase system in diabetes and other age-related diseases. *Clin. Sci.* . **128**, 839–861 (2015).

9.   Nagaraj, Sarkar, Mally, Biemel, … on chemical modification of proteins by carbonyls in diabetic rats: characterization of a major product from the reaction of pyridoxamine and methylglyoxal. *Arch. Biochem.* (available at https://www.sciencedirect.com/science/article/pii/S000398610200067X).

10. Kim, Oi, Kim, Yokozawa, Protective effect of lipoic acid against methylglyoxal-induced oxidative stress in LLC-PK1 cells. *J. Nutr. Sci. Vitaminol.* (available at https://www.jstage.jst.go.jp/article/jnsv/54/1/54_1_99/_article/-char/ja/).

11. K. M. Abdullah, F. A. Qais, I. Ahmad, I. Naseem, Inhibitory effect of vitamin B3 against glycation and reactive oxygen species production in HSA: An in vitro approach. *Arch. Biochem. Biophys.* **627**, 21–29 (2017).

12. P. J. Thornalley, I. Jahan, R. Ng, Suppression of the accumulation of triosephosphates and increased formation of methylglyoxal in human red blood cells during hyperglycaemia by thiamine in vitro. *J. Biochem.* **129**, 543–549 (2001).

13. R. S. Tupe, N. Bangar, A. Nisar, A. Kulkarni, N. Sankhe, R. Chauhan, N. Mistry, S. Shaikh, Piperine exhibits preventive and curative effect on erythrocytes membrane modifications and oxidative stress against in vitro albumin glycation. *J. Food Biochem.*, e13846 (2021).

14. J. Austin, D. Marks, Hormonal regulators of appetite. *Int. J. Pediatr. Endocrinol.* **2009**, 141753 (2009).

15. E. A. Nillni, Regulation of prohormone convertases in hypothalamic neurons: implications for prothyrotropin-releasing hormone and proopiomelanocortin. *Endocrinology.* **148**, 4191–4200 (2007).

16. X. Liu, Z. Jin, S. Summers, D. Derous, M. Li, B. Li, L. Li, J. R. Speakman, Calorie restriction and calorie dilution have different impacts on body fat, metabolism, behavior, and hypothalamic gene expression. *Cell Reports.* **39** (2022), p. 110835.

17. D. Mousseaux, L. Le Gallic, J. Ryan, C. Oiry, D. Gagne, J.-A. Fehrentz, J.-C. Galleyrand, J. Martinez, Regulation of ERK1/2 activity by ghrelin-activated growth hormone secretagogue receptor 1A involves a PLC/PKC□pathway. *Br. J. Pharmacol.* **148**, 350–365 (2006).

18. F. Hu, Y. Xu, F. Liu, Hypothalamic roles of mTOR complex I: integration of nutrient and hormone signals to regulate energy homeostasis. *Am. J. Physiol. Endocrinol. Metab.* **310**, E994–E1002 (2016).

19. M. Nakazato, N. Murakami, Y. Date, M. Kojima, H. Matsuo, K. Kangawa, S. Matsukura, A role for ghrelin in the central regulation of feeding. *Nature.* **409**, 194–198 (2001).

20. R. Kold-Christensen, M. Johannsen, Methylglyoxal Metabolism and Aging-Related Disease: Moving from Correlation toward Causation. *Trends in Endocrinology & Metabolism.* **31** (2020), pp. 81–92.

21. W. Cai, M. Ramdas, L. Zhu, X. Chen, G. E. Striker, H. Vlassara, Oral advanced glycation endproducts (AGEs) promote insulin resistance and diabetes by depleting the antioxidant defenses AGE receptor-1 and sirtuin 1. *Proc. Natl. Acad. Sci. U. S. A.* **109**, 15888–15893 (2012).

22. M. Xue, M. Weickert, N. Rabbani, P. Thornalley, 338-OR: Reversal of Insulin Resistance by Resveratrol and Hesperetin Combination in Overweight and Obese Subjects Correlates with Decrease in Expression of Thioredoxin Interacting Protein. *Diabetes.* **70**, 338–OR (2021).

23. P. Kapahi, M. Kaeberlein, M. Hansen, Dietary restriction and lifespan: Lessons from invertebrate models. *Ageing Res. Rev.* **39**, 3–14 (2017).

24. O. Hahn, L. F. Drews, A. Nguyen, T. Tatsuta, L. Gkioni, O. Hendrich, Q. Zhang, T. Langer, S. Pletcher, M. J. O. Wakelam, A. Beyer, S. Grönke, L. Partridge, A nutritional memory effect counteracts benefits of dietary restriction in old mice. *Nat Metab.* **1**, 1059–1073 (2019).